

ARTICLE

OPEN



4-aminopyridine attenuates inflammation and apoptosis and increases angiogenesis to promote skin regeneration following a burn injury in mice

Rahul V. G.^{1,2}, Govindaraj Ellur^{1,2}, Amir A. Gaber¹, Prem Kumar Govindappa¹✉ and John C. Elfar¹✉

© The Author(s) 2024

Severe thermal skin burns are complicated by inflammation and apoptosis, which delays wound healing and contributes to significant morbidity. Diverse treatments demonstrate limited success in mitigating these processes to accelerate healing. Agents that alter cell behavior to improve healing would alter treatment paradigms. We repurposed 4-aminopyridine (4-AP), a drug approved by the US FDA for multiple sclerosis, to treat severe burns in mice (10-week-old C57BL/6 J male mice weighing 25 ± 3 g). We found that 4-AP, in the early stages of burn healing, significantly reduced the expression of pro-inflammatory cytokines IL1 β and TNF α while increasing the expression of anti-inflammatory markers CD206, ARG-1, and IL10. We demonstrated increased intracellular calcium effects of 4-AP through Orai1-pSTAT6 signaling, where 4-AP significantly mitigated inflammatory effects by promoting M2 macrophage differentiation in in-vitro macrophages and post-skin burn tissues. 4-AP attenuated apoptosis, with decreases in apoptotic markers BAX, caspase-9, and caspase-3 and increases in anti-apoptotic markers BCL2 and BCL-XL. Furthermore, 4-AP promoted angiogenesis through increases in the expression of CD31, VEGF, and eNOS. Together, these likely contributed to accelerated burn wound closure, as demonstrated in increased keratinocyte proliferation (K14) and differentiation (K10) markers. In the later stages of burn healing, 4-AP increased TGF β and FGF levels, which are known to mark the transformation of fibroblasts to myofibroblasts. This was further demonstrated by an increased expression of α -SMA and vimentin, as well as higher levels of collagen I and III, MMP 3, and 9 in mice treated with 4-AP. Our findings support the idea that 4-AP may have a novel, clinically relevant therapeutic use in promoting burn wound healing.

Cell Death Discovery (2024)10:428; <https://doi.org/10.1038/s41420-024-02199-6>

INTRODUCTION

Skin burns most often result from exposure to hot solids and liquids, flames, chemicals, radiation, and other sources of heat [1]. The American Burn Association (ABA) reports that approximately 486,000 patients suffer from burn injuries annually, resulting in a total cost of \$ 42.4 billion [2, 3]. Thermal burns account for about 86% of burns, with direct solid-object contact causing 9% of these burns [4]. The pathophysiological changes caused by thermal burns are complex and vary depending on burn type and severity [5]. Severe burns (third degree) damage the skin's structural integrity, leading to increased inflammation, apoptosis, and reduced oxygen supply with inadequate tissue perfusion [6].

The immune response to a severe burn injury comprises the initial proinflammatory reaction, which is followed by an anti-inflammatory resolution phase. These phases determine the size and severity of the wound [7]. Macrophages are primary immune cells of the skin and they play a vital role in burn injury via the transformation from M1 (pro-inflammatory) to M2 (reparative) phenotypes, which improves angiogenesis and helps to control inflammation – a key driver of local cell death and burn expansion [8]. Inefficient control of inflammation is the

primary driver of secondary burn-wound progression, impaired tissue regeneration and delayed healing [9]. Several studies demonstrated that depletion of dermal macrophages during wound healing has a detrimental impact on wound closure. These macrophage deficient or depleted models feature decreased vessel density, decreased fibroblast to myofibroblast differentiation, and delayed re-epithelialization [10–13]. Few current treatments address these processes and much of current burn care is focused on metabolic and fluid support, as well as infection control [14]. Ideal therapies would increase tissue protection by protecting burned tissue from the effects of inflammation and cell death to bolster oxygenation. This would improve healing, decrease secondary burn progression and reduce the morbidity and mortality associated with severe burns.

4-aminopyridine (4-AP), a potassium channel blocker and calcium channel agonist, is an FDA-approved treatment used for multiple sclerosis and chronic neurodegenerative conditions [15]. We recently found that 4-AP treatment enhanced wound healing and hair follicle regeneration by augmenting keratinocyte, fibroblast, and Schwann-cell function in a splinted full-thickness skin wound model [16]. In addition to pursuing an

¹Department of Orthopaedics and Sports Medicine, University of Arizona College of Medicine, Tucson, AZ 85724, USA. ²These authors contributed equally: Rahul V. G., Govindaraj Ellur. ✉email: pkgovindappa@gmail.com; openelfar@gmail.com

Received: 3 July 2024 Revised: 23 September 2024 Accepted: 27 September 2024
Published online: 04 October 2024

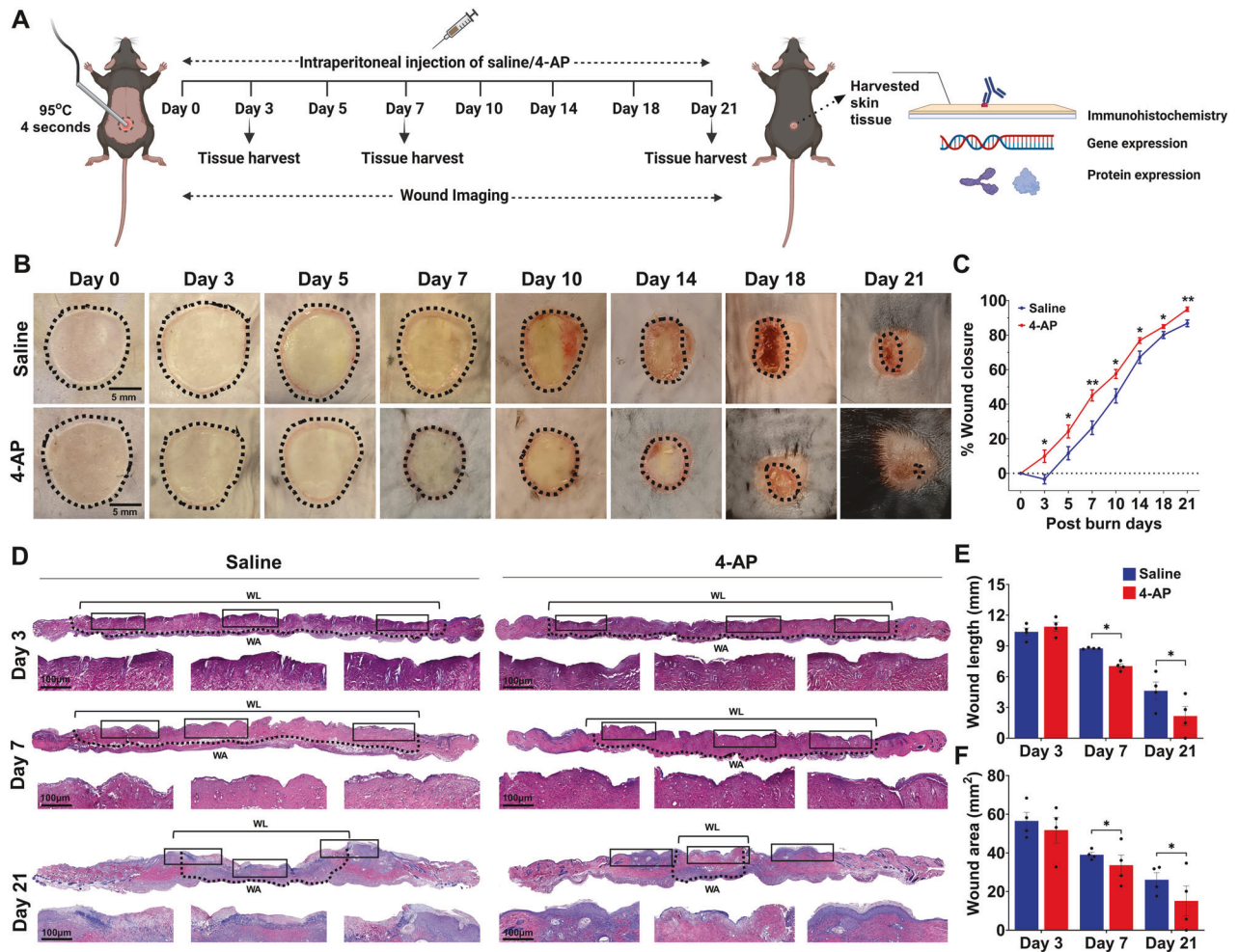


Fig. 1 4-AP expedited burn injury closure and enhanced skin regeneration. A Schematic illustration of experimental design to test the beneficial therapeutic effect of 4-AP in the C57BL/6 mouse burned model. **B** Representative digital images of burn healing in saline and 4-AP (2 mg/kg/IP, single dose immediately after surgery and until day 21) treated mice at 0, 3, 5, 7, 10, 14, 18, and 21 days post-burning. Scale bar = 5 mm. **C** Percent burn wound closure at each time point relative to the initial burn wound area in control and 4-AP-treated mice. $n = 6$ animals per group, with one burn wound per animal. **D** Representative images of H&E-stained sections of full-thickness burn of saline and 4-AP treated skin tissue on days 3, 7, and 21. Scale bar = 100 μ m, $n = 4$ skin tissues per group. **E, F** Quantification of burn wound length and area in H&E-stained skin burn sections using ImageJ software on days 3, 7, and 21. $n = 4$ skin tissues per group. Data are represented as mean \pm SEM. The statistical significance is indicated by asterisks (* $P < 0.05$, and ** $P < 0.0021$ vs. saline group) and compared using two-tailed, unpaired t-tests.

approved clinical trial in human wounds [17], these findings motivated us to study the effects of 4-AP in a standard burn model where we could study 4-AP's effects on secondary burn progression. Studies have shown the role of the Orai1 (Orai calcium release-activated calcium modulator 1) calcium channel in maintaining skin homeostasis and promoting wound healing [18, 19]. However, its impact on skin burns is unknown. We hypothesized that 4-AP attenuates early inflammation through Orai1-pSTAT6 signaling and apoptosis, potentially leading to accelerated angiogenesis, which helps to prevent secondary burn progression and accelerate burn closure. Therefore, our investigation focused on examining the effects of 4-AP on inflammation, apoptosis, angiogenesis, extracellular matrix (ECM) remodeling, and cellular phenotypic changes in keratinocytes, macrophages, and fibroblasts.

We found that 4-AP reduced early inflammation via Orai1-pSTAT6 signaling and reduced apoptosis. 4-AP also enhanced angiogenesis to expedite burn closure, ECM regeneration, and remodeling. Our data supports a novel therapeutic application of 4-AP in promoting cutaneous burn healing, which is clinically translatable.

RESULTS

4-AP expedited burn injury closure and enhanced skin regeneration following skin burn

Mouse burn models are commonly used to evaluate tissue regeneration and repair [20]. To test the hypothesis that systemic 4-AP treatment promotes burn wound closure and healing, we created a 10-mm-diameter heat-induced, severe, full-thickness skin burn on the dorsal thoracolumbar surface of mice. Approved burn model experimental details are shown in Fig. 1A. Macroscopic imaging burns (Fig. 1B) allowed the assessment of burn closure percentage over time (Fig. 1C; * $P < 0.05$ and ** $P < 0.0021$) revealed accelerated burn closure in 4-AP-treated mice compared to saline controls. Accelerated healing was attributable to early protection against secondary expansion of burn injury with 4-AP treatment, evidenced as the difference at day 3 post burn injury where 4-AP treated animals closed 9.87% of their burn area, whereas saline treated animals expanded their wounds an average of 3.39% (average % wound closure difference was 13.26%, * $P < 0.05$). Thereafter, burn closure in the 4-AP group consistently outpaced saline controls on day 5 (24.24% vs. 11.61%), day 7 (45.09% vs. 26.38%), day 10 (57.48% vs. 44.76%), day 14 (76.86% vs. 67.17%), day 18 (84.92% vs. 80.06%),

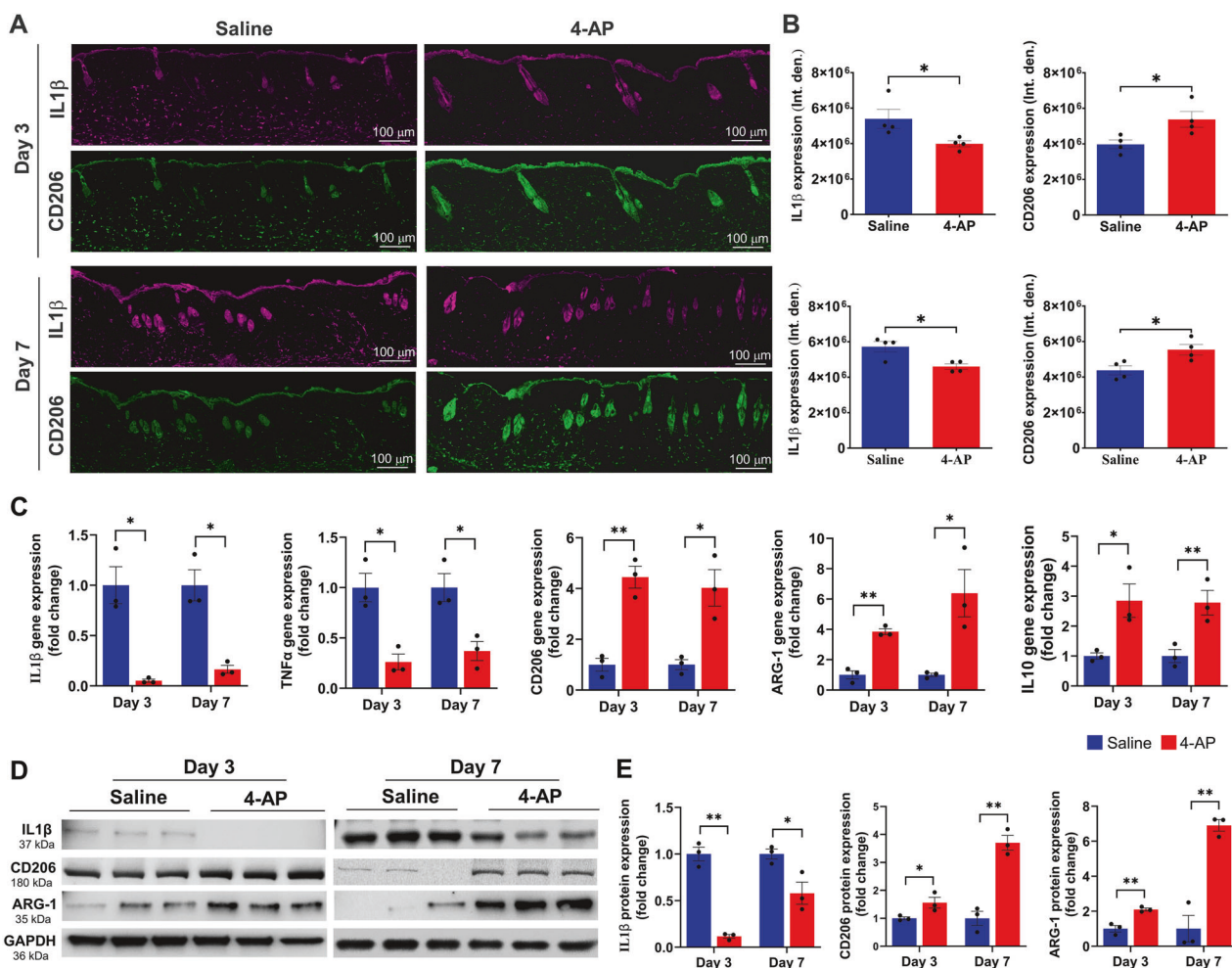


Fig. 2 4-AP attenuated pro-inflammation and accelerated anti-inflammatory effects following skin burn. A, B Representative images of IF staining of IL1 β (pro-inflammatory) and CD206 (anti-inflammatory) and its quantitative results where 4-AP significantly controlled inflammatory resolution compared to saline-treated skin burn tissues on days 3 and 7. Scale bar = 100 μ m. $n = 4$ skin tissues per group. **C** qRT-PCR data shows that 4-AP treatment significantly attenuated pro-inflammatory genes (IL1 β and TNF α ; M1 macrophage markers) and upregulated anti-inflammatory genes (CD206, ARG-1, and IL10; M2 macrophage markers) compared to the saline group on days 3 and 7. $n = 3$ skin tissues per group. **D, E** Western blotting images and quantitative results show that 4-AP treatment significantly attenuated IL1 β and upregulated CD206 and ARG-1 protein expressions compared to the saline group on days 3 and 7. $n = 3$ skin tissues per group. Data are represented as mean \pm SEM, and the statistical significance is indicated by asterisks (* $P < 0.05$ and ** $P < 0.0021$ vs. saline group) and compared using two-tailed, unpaired t-tests.

and day 21 (94.96% vs. 86.80%). By day 21, 4-AP treated animals had all healed, while the saline-treated animals had not. The dermis area and dermal length (distance between healing epidermal tongues) were measured using H&E histology (Fig. 1D). Quantitative analysis of burn wound length (Fig. 1E; * $P < 0.05$) on day 7 (7.03 mm vs. 8.75) and day 21 (2.15 mm vs. 4.64 mm) and burn wound area (Fig. 1F; * $P < 0.05$) on the same days (33.62 mm 2 vs. 39.03 mm 2 and 15.14 mm 2 vs. 26.11 mm 2) confirmed that 4-AP accelerates tissue healing compared to saline. Compared to saline, 4-AP treatment resulted in significant differences in the structural organization of the epidermis and dermis, which was likely attributable to the proliferation, migration, and transformation of keratinocytes, immune cells, and fibroblasts. There was a considerable effect on accelerating granulation, re-epithelialization, and burn wound-healing closure rate in 4-AP treated animals.

4-AP attenuated inflammation and augmented anti-inflammatory effects following skin burn

We aimed to test 4-AP's effect on post-burn inflammation, which is the earliest response to burn injury, lasting for weeks

depending on burn severity [21]. Inflammation causes keratinocytes and fibroblasts release factors that attract inflammatory macrophages and stimulate angiogenesis [22]. The quantitative results of the macrophage IF analysis showed that 4-AP treatment significantly shifted macrophage polarization from the M1 (IL1 β ; Inflammatory) to M2 (CD206; Reparative) phenotype in tissues abutting the burn site on days 3, and 7 (Fig. 2A, B; * $P < 0.05$). These data suggest a role for 4-AP in activation and recruitment of macrophages. 4-AP treatment also significantly decreased pro-inflammatory genes (IL1 β and TNF α), and increased the expression of anti-inflammatory genes (CD206, ARG-1, and IL10) compared to the saline group (Fig. 2C; * $P < 0.05$ and ** $P < 0.0021$). These changes were also evident at the protein expression level, with 4-AP significantly attenuating IL1 β expression, while increasing expression of CD206, and ARG-1 proteins compared with saline treatment (Fig. 2D, E; * $P < 0.05$ and ** $P < 0.0021$). Taken together, these results suggest a key role for 4-AP treatment in modulating inflammatory resolution in skin burns, with possible beneficial effects on early angiogenesis.

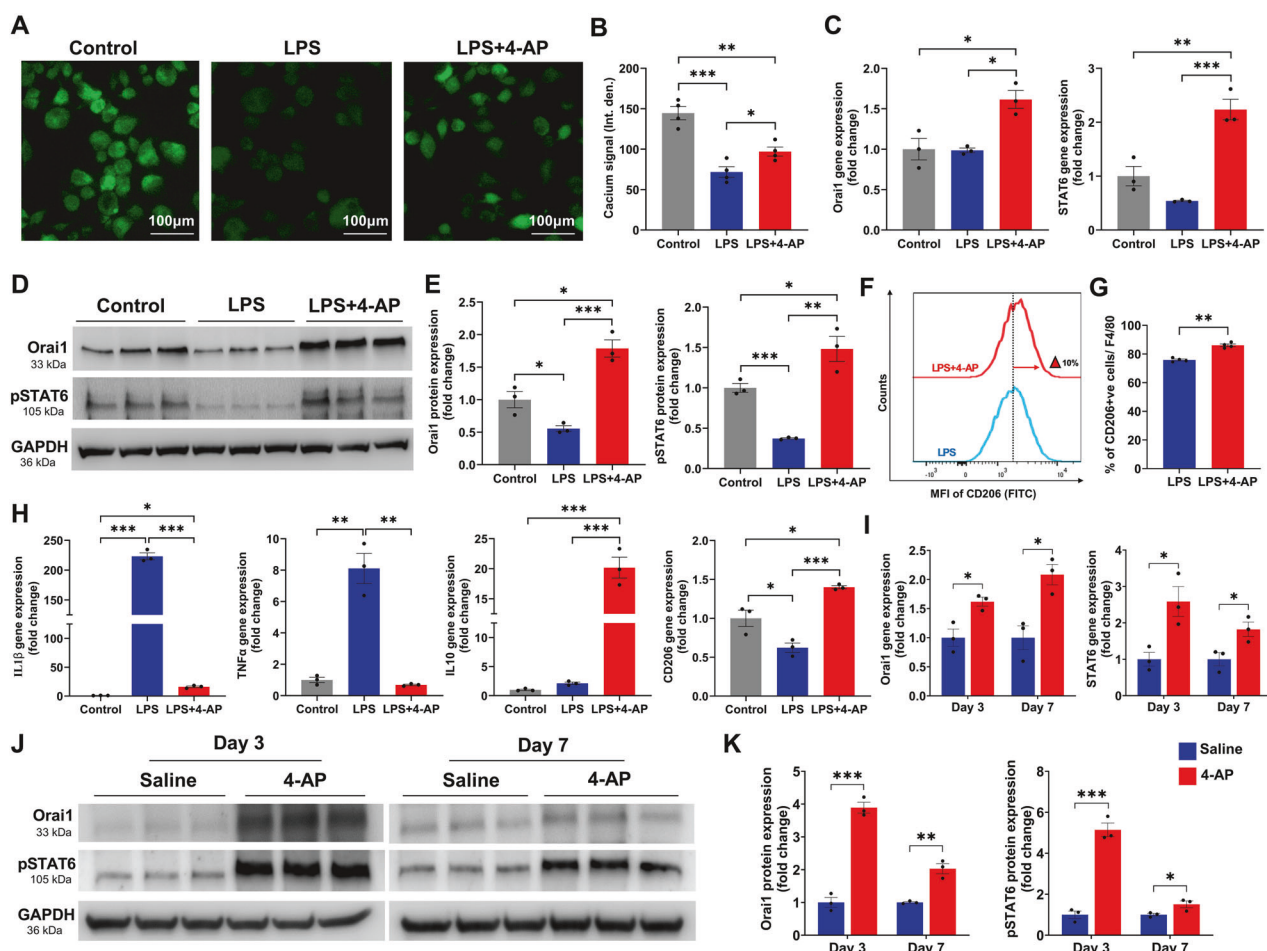


Fig. 3 4-AP augmented macrophage reparative function via Orai1 calcium channel signaling. **A, B** Representative images and quantitative results of IF staining of calcium signaling in control, LPS, and LPS + 4-AP treated mouse bone marrow-derived macrophages (BMMØs) at 24 h. Scale bar = 100 μ m. $n = 4$ per group. **C** qRT-PCR data shows that LPS + 4-AP treatment significantly increased the expression of Orai1 and STAT6 in BMMØs compared to the LPS and control groups. $n = 3$ per group. **D, E** Western blotting images and quantitative results showed that LPS + 4-AP treatment significantly increased Orai1 and STAT6 protein expressions in BMMØs compared to the LPS and control groups. $n = 3$ per group. **F, G** Representation of flow cytometry histogram and a quantitative result of percent CD206 $^{+ve}$ macrophages gated against F4/80 $^{+ve}$ cells in LPS versus LPS + 4-AP treated groups. $n = 3$ per group. **H** qRT-PCR data shows that 4-AP treatment significantly attenuated pro-inflammatory genes (IL1 β and TNF α) and augmented anti-inflammatory genes (IL10 and CD206) in BMMØs under LPS stress conditions. $n = 3$ per group. **I** qRT-PCR data shows that 4-AP treatment significantly increased expression of Orai1 and STAT6 genes in 4-AP treated skin burn tissues on days 3 and 7. $n = 3$ skin tissues per group. **J, K** Western blotting images and quantitative results show that 4-AP treatment significantly increased Orai1 and STAT6 protein expressions compared to the saline group on days 3 and 7. $n = 3$ skin tissues per group. Data are represented as mean \pm SEM. The statistical significance is indicated by asterisks (* $P < 0.05$, ** $P < 0.0021$, and *** $P < 0.0002$ vs. control/LPS/saline group) and compared using two-tailed, unpaired t-tests for two groups and ordinary one-way ANOVA for three groups.

4-AP augmented macrophage reparative function via Orai1 calcium channel signaling

Recent studies showed that Orai1 is a calcium channel that plays a crucial role in M1 to M2 macrophage differentiation and its reparative functions [23, 24]. We aimed to investigate whether 4-AP acts as a calcium agonist through Orai1 downstream signaling in macrophage cells to enhance the anti-inflammatory function in the setting of in-vitro lipopolysaccharide (LPS)-induced inflammatory stress and in-vivo-skin burn injury. We first conducted an MTT assay to determine the percentage of viable cells at different 4-AP concentrations and selected based on clinically relevant 4-AP plasma concentrations [25, 26]. We found that 4-AP treatment ranging from 1 nM to 100 μ M did not affect the viability of mouse bone marrow-derived macrophages (BMMØs) at 24 h (Supplementary Fig. S1), with significantly higher concentrations resulting in toxicity. Based on these findings, we selected 1 μ M of 4-AP as an effective treatment dose for further in-vitro cell-culture experiments. We then tested 4-AP's effect on

intracellular calcium expression in BMMØs and found that it significantly increased the expression of calcium under LPS stress conditions (Fig. 3A, B; * $P < 0.05$). The LPS alone group showed a considerably decreased expression as compared to the 4-AP treatment and control groups (Fig. 3A, B; * $P < 0.05$ and *** $P < 0.0002$). Next, we tested 4-AP's effect on Orai1-pSTAT6 downstream signaling for anti-inflammatory effects. 4-AP significantly increased gene expression of Orai1 and STAT6 as compared to LPS and untreated cells (Fig. 3C; * $P < 0.05$, ** $P < 0.0021$, and *** $P < 0.0002$ vs. control/LPS/saline group) and compared using two-tailed, unpaired t-tests for two groups and ordinary one-way ANOVA for three groups.

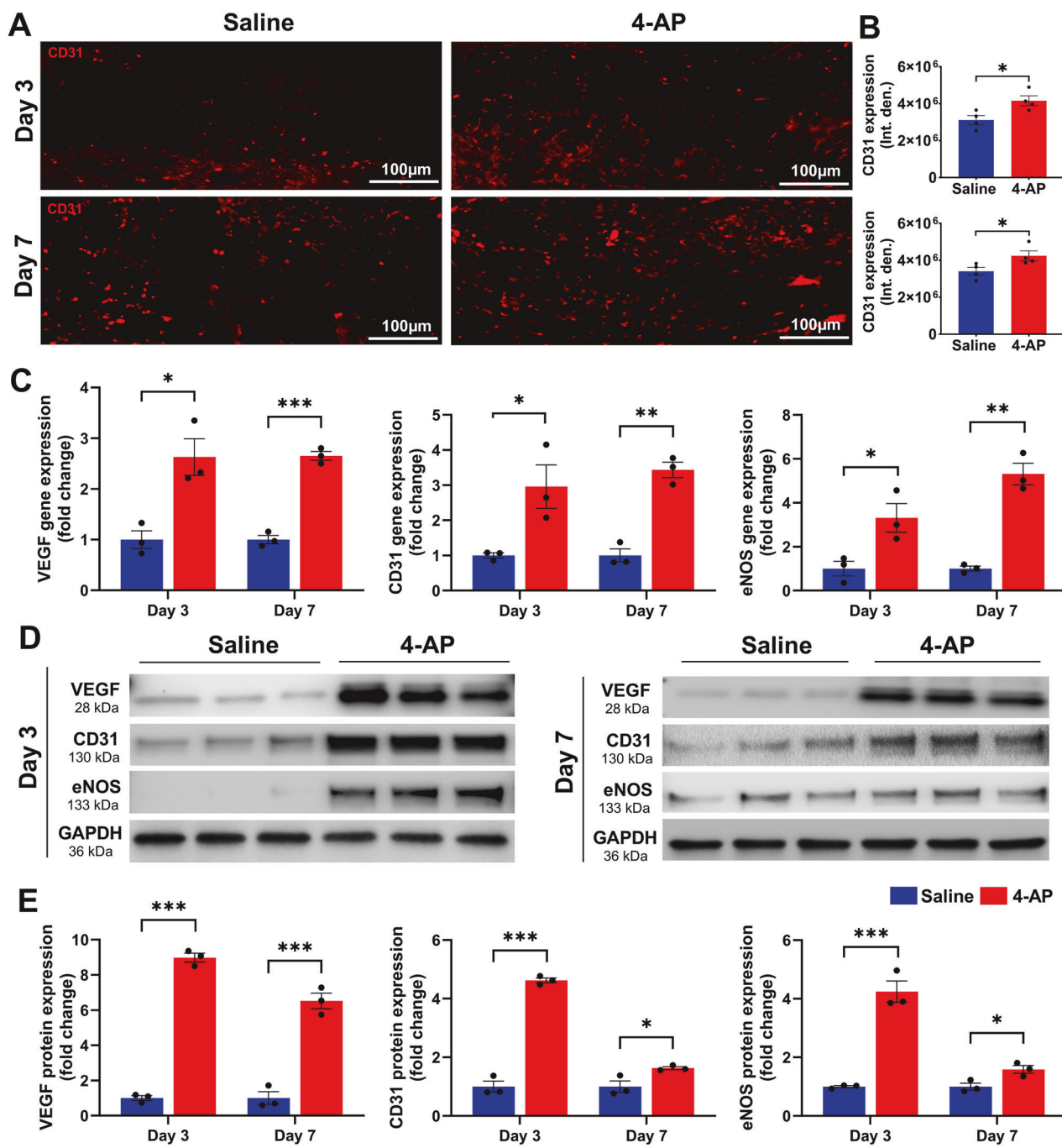


Fig. 4 4-AP enhanced angiogenesis following skin burn. **A, B** Representative images and quantitative results of IF staining of CD31 in saline and 4-AP treated skin burn tissues on days 3 and 7. Scale bar = 100 μ m. $n = 4$ skin tissues per group. **C** qRT-PCR data shows that 4-AP treatment significantly increased the expression of angiogenesis genes (VEGF, CD31, and eNOS) compared to the saline group on days 3 and 7. $n = 3$ skin tissues per group. **D, E** Western blotting images and quantitative results showed that 4-AP treatment significantly increased angiogenesis protein expressions (VEGF, CD31, and eNOS) compared to the saline group on days 3 and 7. $n = 3$ skin tissues per group. Data are represented as mean \pm SEM. The statistical significance is indicated by asterisks (* $P < 0.05$, ** $P < 0.0021$, and *** $P < 0.0002$ vs. saline group) and compared using two-tailed, unpaired t-tests.

genes (IL10, CD206, and VEGF), indicating Orai1-pSTAT6 signaling effect on M1 to M2 macrophage differentiation under LPS stress conditions (Fig. 3H and Supplementary Fig. S2; * $P < 0.05$, ** $P < 0.0021$, and *** $P < 0.0002$). We then validated these results in skin burn tissues, where 4-AP significantly upregulated both gene (Fig. 3I; * $P < 0.05$) and protein expression of Orai1 and pSTAT6 on post-burn days 3 and 7 (Fig. 3J, K; * $P < 0.05$, ** $P < 0.0021$, and *** $P < 0.0002$). These results and skin burn tissue anti-inflammatory effects complement in-vitro macrophage

findings. In summary, our study supports 4-AP's calcium agonist effects likely via Orai1-pSTAT6 signaling and that this may mitigate inflammatory effects by promoting M2 macrophage differentiation towards the end of improving skin thermal burn healing.

4-AP augmented angiogenesis following skin burn

Revascularization through neo angiogenesis begins immediately after burns and provides vital oxygen and nutrients for healing [27]. Impaired angiogenesis impedes burn wound regeneration

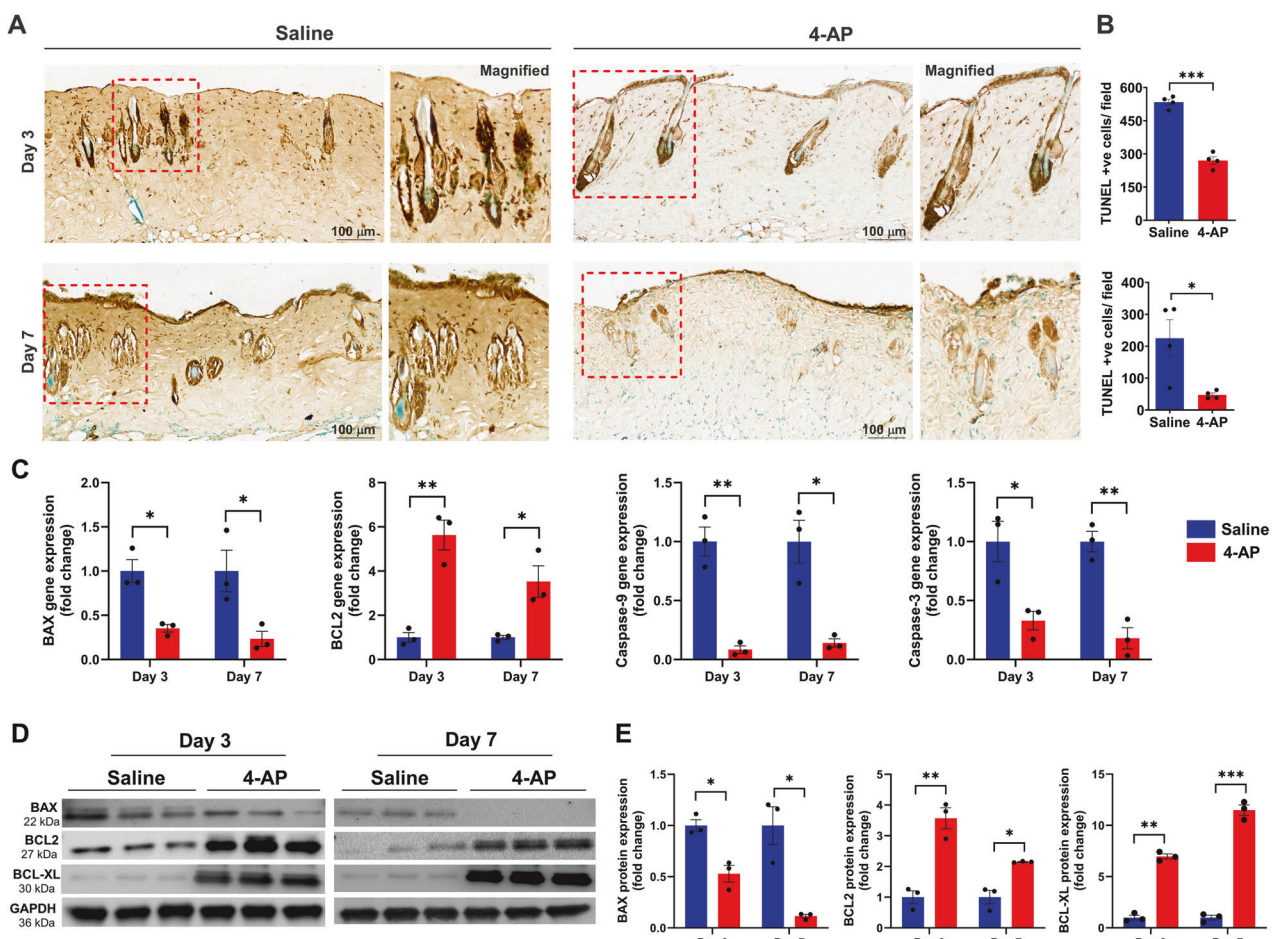


Fig. 5 4-AP attenuated pro-apoptosis and accelerated anti-apoptosis effects following skin burn. **A, B** Representative images of DAB-TUNEL staining of apoptosis and quantitative results of TUNEL positive cells in saline and 4-AP treated skin burn tissues on days 3 and 7. $n = 4$ skin tissues per group. **C** qRT-PCR data shows that 4-AP treatment significantly attenuated pro-apoptosis genes (BAX, caspase-9, and caspase-3) and upregulated anti-apoptosis genes (BCL2) compared to the saline group on days 3 and 7. $n = 3$ skin tissues per group. **D, E** Western blotting images and quantitative results showed that 4-AP treatment significantly attenuated expressions of pro-apoptosis protein (BAX) and upregulated anti-apoptosis proteins (BCL2 and BCL-XL) as compared to the saline group on days 3 and 7. $n = 3$ skin tissues per group. Data are represented as mean \pm SEM. The statistical significance is indicated by asterisks (* $P < 0.05$, ** $P < 0.0021$, and *** $P < 0.0002$ vs. saline group) and compared using two-tailed, unpaired t-tests.

[28], and we tested the hypothesis that 4-AP treatment could enhance angiogenesis early after burns. We found increased CD31 IF staining at days 3 and 7 post burn with 4-AP treatment compared to saline (Fig. 4A, B; * $P < 0.05$). Corresponding changes were found in the gene and protein expression level of several known markers of neo-angiogenesis, including VEGF, CD31, and eNOS with 4-AP treatment (gene expression, Fig. 4C; * $P < 0.05$, ** $P < 0.0021$, and *** $P < 0.0002$; corresponding protein expression Fig. 4D, E; * $P < 0.05$ and *** $P < 0.0002$) as compared to the saline group. Histomorphometric evaluation of tissue specimens confirmed the effects of vascular augmentation with 4-AP treatment, which are crucial for both regeneration and the control of post-burn inflammation and apoptosis.

4-AP attenuated apoptosis and increased anti-apoptosis markers following skin burn

Recent studies showed that burns cause significant apoptosis or cell death, which hinders skin cell regenerative efforts and impedes healing [29, 30]. To investigate the anti-apoptotic effect of 4-AP after a burn injury, we used DAB-TUNEL to stain burned tissues (Fig. 5A). On day 3, 4-AP treatment significantly reduced apoptosis compared to saline treatment (270 vs. 533 per field; Fig. 5A, B; *** $P < 0.0001$). By day 7, 4-AP treatment

continued to show protective effects (vs. day 3, 4-AP treatment) against apoptosis (47 vs. 270 per field; Fig. 5A, B; * $P < 0.05$) compared to saline treatment (47 vs. 224 per field; Fig. 5A, B; * $P < 0.05$). On days 3 and 7 post injury, saline-treated mice showed noticeable apoptosis in the skin hair follicles and the epidermis (keratinocytes) and dermis (fibroblasts) regions (Fig. 5A; magnified field), whereas 4-AP treatment resulted in significantly reduced apoptosis and increased regeneration of new cells in these regions and in hair follicle bulges (green cells). Treatment with 4-AP attenuated the gene expression of pro-apoptosis (BAX, caspase-9, and caspase-3) and bolstered the expression of anti-apoptosis (BCL2) (Fig. 5C; * $P < 0.05$ and ** $P < 0.0021$) and this also led to corresponding changes at protein levels (Fig. 5D, E; * $P < 0.05$, ** $P < 0.0021$, and *** $P < 0.0002$) on days 3 and 7 post-burn injury. This significant positive effect of 4-AP on preventing apoptosis and augmenting anti-apoptosis may be the basis for the accelerating functional burn wound closure after burn injury.

4-AP accelerated re-epithelialization following skin burn

Re-epithelialization is crucial for providing a new barrier between deeper exposed tissues and the bacteria-laden outside environment [31]. Several studies show that keratin markers K10

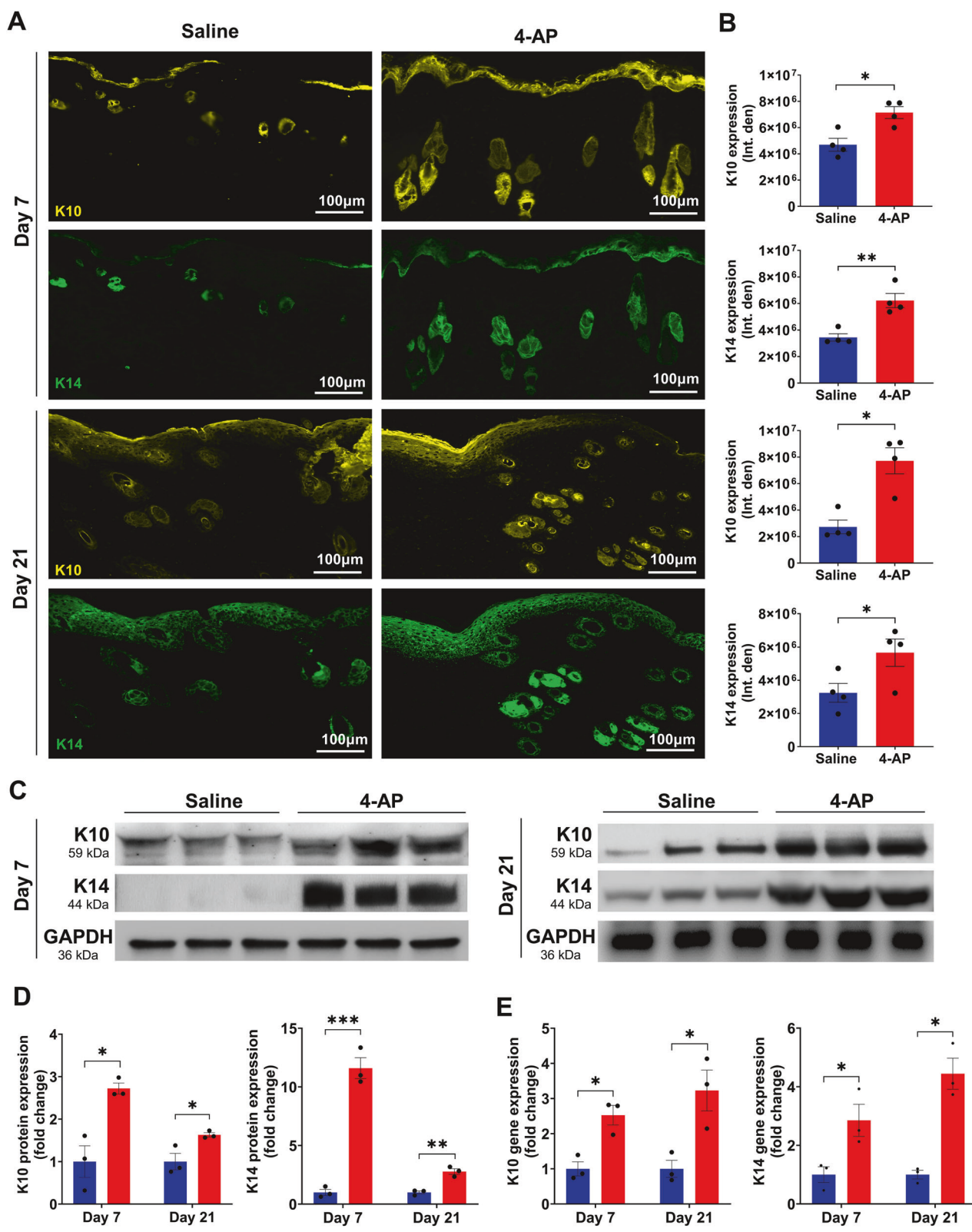


Fig. 6 4-AP accelerated epithelization and keratinocytes terminal differentiation following skin burn. A, B Representative images and quantitative results of IF staining of keratinocyte markers (K10; terminal differentiation and K14; proliferative) in saline and 4-AP treated skin burn tissues on days 3 and 7. Scale bar = 100 μ m. n = 4 skin tissues per group. **C, D** Western blotting and (E) qRT-PCR quantitative results show that 4-AP treatment significantly increased keratin markers protein and gene (K10 and K14) expressions compared to the saline group on days 3 and 7. n = 3 skin tissues per group. Data are represented as mean \pm SEM. The statistical significance is indicated by asterisks (*P < 0.05, **P < 0.0021, and ***P < 0.0002 vs. saline group) and compared using two-tailed, unpaired t-tests.

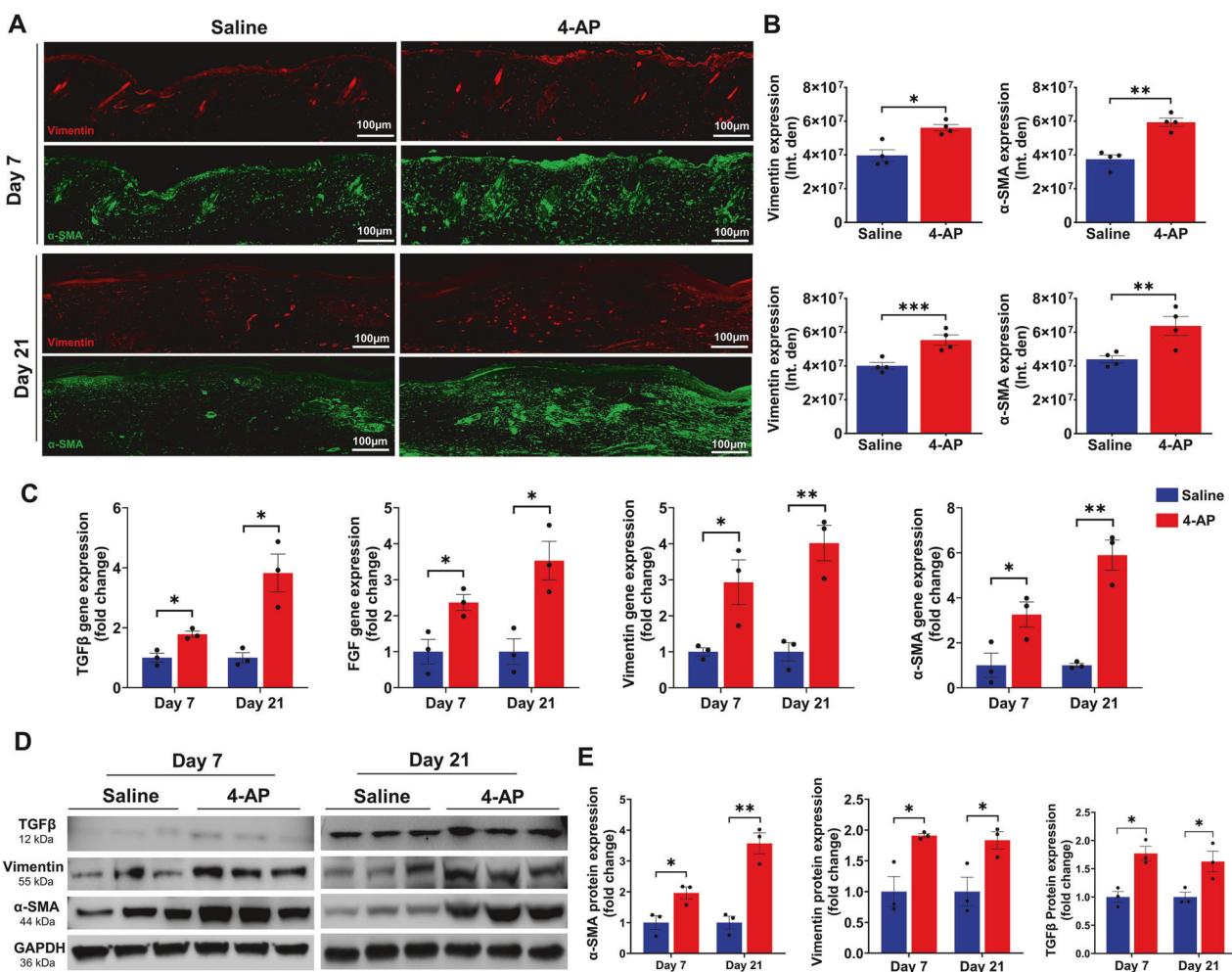


Fig. 7 4-AP increased fibroblast to myofibroblast transformation following skin burn. A, B Representative images and quantitative results of IF staining of vimentin (fibroblasts) and α -SMA (myofibroblasts) in saline and 4-AP treated skin burn tissues on days 3 and 7. Scale bar = 100 μ m. $n = 4$ skin tissues per group. **C** qRT-PCR data shows that 4-AP treatment significantly increased the expression of TGF β , vimentin, α -SMA, and FGF genes compared to the saline group on days 7 and 21. $n = 3$ skin tissues per group. **D, E** Western blotting images and quantitative results showed that 4-AP treatment significantly increased the expression of TGF β , vimentin, and α -SMA proteins compared to the saline group on days 7 and 21. $n = 3$ skin tissues per group. Data are represented as mean \pm SEM. The statistical significance is indicated by asterisks (* $P < 0.05$, ** $P < 0.0021$, and *** $P < 0.0002$ vs. saline group) and compared using two-tailed, unpaired t-tests.

(terminal differentiation), and K14 (undifferentiation) are expressed in both epidermis and regenerating hair follicles [32, 33]. Given our observations that 4-AP increased the thickness of healing epidermal tongues after burns as well as improved dermal regeneration, we sought to investigate whether these observations were linked to an increased expression of these same markers in keratinocytes and whether there were changes in epidermal differentiation. IF staining analysis of keratin markers showed that 4-AP treatment significantly increased the expression of K10, and K14 in both epidermis and hair follicles on days 7, and 21 compared to the saline group (Fig. 6A, B; * $P < 0.05$ and ** $P < 0.0021$). There was no significant difference in the IF expression of these markers on day 3 (data not shown), as would be expected as skin healing follows wound inflammation. We focused on gene and protein expression of these markers in burned skin tissues on days 7 and 21 and found that 4-AP treatment significantly increased both protein (Fig. 6C, D; * $P < 0.05$ and *** $P < 0.0002$) and gene (Fig. 6E; * $P < 0.05$) expression of K10 and K14. This was highly suggestive of positive effects on re-epithelialization for 4-AP reminiscent of effects we observed in standard wound healing [16].

4-AP promoted fibroblast to myofibroblast transformation following skin burn

TGF- β plays a central role in the transition of fibroblasts (vimentin-positive cells) to myofibroblasts (α -SMA-positive cells), which is a crucial step in skin burn healing [34, 35]. Fibroblasts, along with macrophages (immune cells), endothelial cells (vessels), and keratinocytes are all components of tissue granulation, where myofibroblasts play a crucial role in accelerating burn wound contraction, and ECM production [36]. Given our finding of 4-AP's effects on the generation of M2 macrophages, angiogenesis, and keratinocytes in the burn wound tissues, we sought to investigate effects on the transformation of fibroblasts following burn injury on days 7 and 21. The results of IF staining showed that 4-AP significantly increased the expression of both vimentin and α -SMA positive cell types (Fig. 7A, B; * $P < 0.05$, ** $P < 0.0021$, and *** $P < 0.0002$), which is evident on day 21. Next, we investigated the effects of 4-AP on vimentin, α -SMA, FGF, and TGF β markers at the gene levels, where 4-AP notably increased the expression of all these gene markers (Fig. 7C; * $P < 0.05$ and ** $P < 0.0021$) and protein expression (vimentin, α -SMA, and TGF β proteins: Fig. 7D, E; * $P < 0.05$ and ** $P < 0.0021$) compared with saline treatment. Our

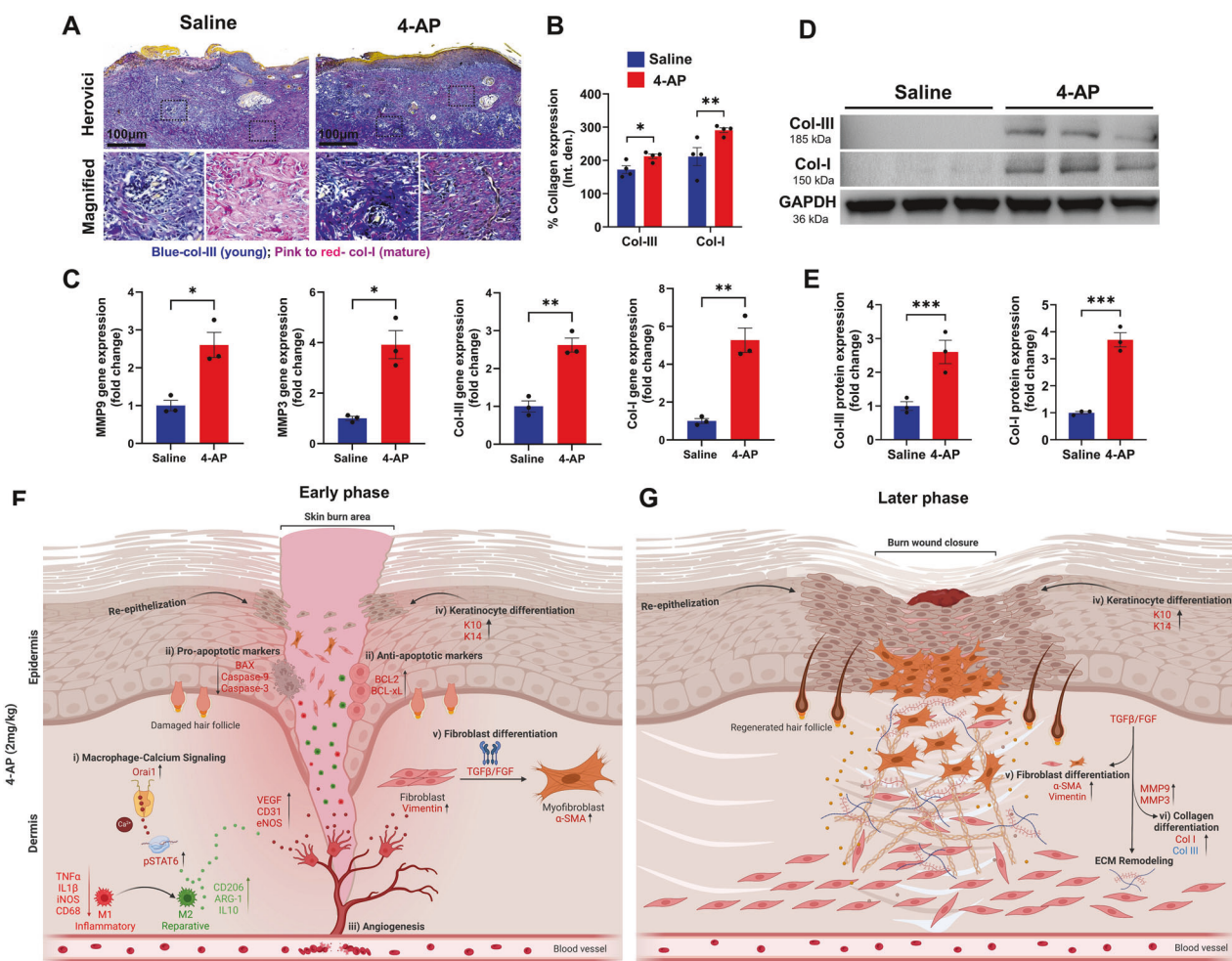


Fig. 8 4-AP advanced skin burns wound repair by increasing collagen and MMP expressions. **A, B** Representative images and quantitative results of Herovici's staining of collagen III/I in saline and 4-AP treated skin burn tissues on days 7 and 21. $n = 4$ skin tissues per group. **C** qRT-PCR data shows that 4-AP treatment significantly increased the expression of collagen-III/I and MM9/3 genes compared to the saline group on days 7 and 21. $n = 3$ skin tissues per group. **D, E** Western blotting images and quantitative results showed that 4-AP treatment significantly increased collagen-III/I protein expressions compared to the saline group on day 21. $n = 3$ skin tissues per group. Data are represented as mean \pm SEM. The statistical significance is indicated by asterisks (* $P < 0.05$, ** $P < 0.0021$, and *** $P < 0.0002$ vs. saline group) and compared using two-tailed, unpaired t-tests. Schematic illustration of early (**F**) and late (**G**) phases of skin burn healing. 4-AP expedites burn wound healing via controlling multi-cellular events of (i) macrophage, (ii) apoptosis, (iii) angiogenesis, (iv) keratinocyte, and (v) fibroblast. During the early phase (days 3 and 7) of burn wound healing, 4-AP significantly mitigates inflammation via Orai1-pSTAT6 signaling and apoptosis and enhances angiogenesis, keratin, and fibroblast differentiation. In the later phase (day 21), 4-AP promotes wound closure by accelerating the remodeling of the ECM via stimulating fibroblast and collagen differentiation.

data supported a vital role for 4-AP treatment on TGF β downstream signaling for burn tissue remodeling.

4-AP augmented matrix remodeling and tissue healing following skin burn

Later in skin healing after a burn, fibroblasts, keratinocytes, and immune cells play a crucial role in remodeling the ECM [37]. These cells, especially fibroblasts, produce ECM proteins such as collagen types III and I and release matrix metalloproteinases (MMPs) [38]. MMPs such as MMP3 and MMP9 are responsible for synthesis and degradation of ECM, including collagen [39, 40]. While healing, the production of type III collagen (early immature collagen product) increases, providing elasticity and resilience, while type I collagen (late mature collagen product) provides tensile strength [41, 42]. We quantified the amounts of collagen I and III, as well as the expression of MMP9 and MMP3 on day 21. The results of the Herovici's (collagen) staining showed that 4-AP significantly increased the expression of both collagen III and I (Fig. 8A, B; * $P < 0.05$ and ** $P < 0.0021$). 4-AP's effect on gene expression of

collagen I, collagen III, MMP3 and MMP9 were all increased compared with saline (Fig. 8C; * $P < 0.05$ and ** $P < 0.0021$), and this was true for protein expression of collagen I and III proteins (Fig. 8D, E; *** $P < 0.0002$) as well. This supports the idea that 4-AP had a pro-remodeling effect on ECM in healing burns. Schematic illustration of early and late phases of skin burn healing are illustrated in Fig. 8F, G.

DISCUSSION

In previous work, we demonstrated that 4-AP accelerated wound healing in a full-thickness excisional mouse model by augmenting re-epithelialization, dermal regeneration, and reinnervation [16]. The effects we previously found were on multiple cell types, and were sufficient to satisfy the FDA requirements to pursue a trial through exemption on healthy patients with standard skin-punch biopsy wounds [17]. The effects on standard full-thickness wounds could not, however, be translated directly to an understanding of the 4-AP's effects on thermal burns. Here we aimed to investigate,

for the first time, whether 4-AP does indeed attenuate inflammation and apoptosis by enhancing angiogenesis in actual severe burns, and whether this would translate to accelerated burn wound closure. Our data showed that 4-AP treatment significantly attenuated inflammation and apoptosis, and enhanced angiogenesis and epidermal and dermal regeneration to accelerate burn wound closure.

After a burn injury, skin responses to the heat injury are critical to mitigating burn wound expansion and initiating tissue regeneration. We first focused on the impact of heat-induced burns on the skin, specifically looking at pro-inflammatory and macrophage responses and the role of 4-AP in controlling these factors. Burn injuries primarily cause inflammation, which can worsen if M1 macrophage phenotypes dominate over M2 macrophage populations [8, 43]. This exacerbates inflammation and leads to cell death in the burn wounds [44]. The timely transformation of M1 to M2 macrophages is crucial for reducing inflammation, and supporting the release of growth factors to bolster angiogenesis [45]. Recent studies have indicated that the Orai1 calcium channel, activated by STIM (stromal interaction molecule), plays a crucial role in controlling skin homeostasis and inflammation through macrophage differentiation [19, 46, 47]. Our results showed that 4-AP enhances the anti-inflammatory effects of Orai1-pSTAT6 downstream signaling in burned skin tissue and macrophages under LPS-induced stress. Notably, other studies suggest that macrophages lacking Orai1 exhibit reduced expression of anti-inflammatory cytokines [23, 24]. Therefore, our findings, in conjunction with other studies, underscore the significance of Orai1 in skin healing. Several studies also suggest that depletion of macrophages results in defective wound repair [10–13, 48], likely through the functional impairment of cytokines and growth factors, such as epidermal growth factor (EGF), keratinocyte growth factor (KGF), transforming growth factor- β (TGF β), vascular endothelial growth factor (VEGF), and others [49, 50]. These factors activate the proliferation and maturation of different cell types, especially keratinocytes, fibroblasts, and endothelial cells. This complex transformation contributes to burn wound granulation, re-epithelialization, and ECM repair. Our data suggests that 4-AP may accelerate burn wound closure by accelerating these transitions.

Burn injury-induced ischemia drives angiogenesis, which plays a critical role in tissue repair and regeneration [51] by providing nutrients and oxygenation to ischemic tissues [52] as well as facilitating the ingress of inflammatory neutrophils and macrophages to granulate the wound bed [53]. Unsuccessful re-vascularization of burned tissues impedes the resolution of inflammation in burned tissue [54]. VEGF is a potent mediator of angiogenesis and promotes cell migration, proliferation, and permeability. VEGF activates eNOS through AKT phosphorylation, which in turn helps produce nitric oxide (NO) to regulate vasodilation and permeability [55, 56]. Several studies highlight the significance of VEGF in wound healing in both in-vitro and in-vivo settings [51, 57]. CD31 is highly expressed in endothelial cells and can be used to measure vessel density. 4-AP significantly increased the early post-burn expression of VEGF, eNOS, and CD31 at both the gene and protein levels on days 3 and 7. Our findings suggest that early 4-AP driven angiogenesis may attenuate inflammation through the transformation of M1 to M2 macrophages, and that this may ultimately accelerate burn healing through the transformation of keratinocytes and fibroblasts.

Burns kill epidermal-keratinocytes and dermal fibroblasts, along with hair follicle bulges through activation of inflammation, apoptosis, and necrosis [58]. We found that 4-AP markedly reduced apoptosis (TUNEL-positive cells) and significantly augmented cell proliferation (methyl green-positive cells) in both epidermal and dermal sites of burned skin tissues on days 3 and 7. This suggests an anti-apoptotic role for 4-AP. Burn-induced cell death occurs via the intrinsic pathway (involving BCL2 and related

proteins) and the extrinsic pathway (involving death receptor signaling, e.g., TNF α interacting with TNF receptor 1) [59, 60], which both lead to the activation of caspase-9 and downstream effector caspase-3. Intrinsic apoptosis is initiated internally within the cell via BCL2 family proteins, including both pro-apoptotic (BAX and BAK) and anti-apoptotic (BCL2 and BCXL) proteins, all of which tightly regulate intrinsic mitochondrial-mediated apoptosis [61, 62]. 4-AP treatment significantly reduced pro-apoptosis expression levels including BAX, caspase-9, and caspase-3 while increasing anti-apoptosis expression levels including BCL2 and BCXL. These results support the anti-apoptosis function of 4-AP.

Keratinocytes are the dominant cells of the epidermis and they depend on a vascular network to interact with immune cells and fibroblasts to effect successful healing [63, 64]. Specifically, M2 macrophages secrete several anti-inflammatory, anti-apoptotic, angiogenic, and other growth factors that act on keratinocytes [65] to drive migration, proliferation, and differentiation during re-epithelialization [66, 67]. The K10 marker is expressed in terminally differentiated keratinocytes and in hair follicle stem cells below the epidermis [68, 69], while K14 is associated with proliferative and migratory keratinocytes, as well as new hair follicle stem cells [70, 71]. Our data showed that on days 7 and 21, the expression of both K10 and K14 was significantly higher in the epidermis and dermis in the 4-AP treatment group compared to the saline group. However, this increase was nonsignificant on day 3, suggesting that this effect of 4-AP treatment is consistent with late effects on burn healing. In our previous study using a full-thickness skin excision mouse model, we found 4-AP-mediated effects on the number of hair follicles and the expression of K14, K15, and K17, which are structural markers of hair follicles [16]. This contrasted with our previous understanding of 4-AP as a neurogenic regenerative agent. Notably, we could find no previous studies demonstrated hair follicle regeneration following skin burns. Our current data supports the idea of hair follicle regeneration, and we believe that this effect may be due to either 4-AP's neurogenic effects, or alternatively direct effects on keratinocytes themselves. This will warrant further investigation in future studies.

After a burn, fibroblasts are recruited by activated immune cells to secrete ECM proteins [37, 72] like FGF and TGF β that play a role in the proliferation and differentiation of fibroblasts (vimentin-positive cells) into myofibroblasts (α -SMA-positive cells). The ECM, which makes up over 70% of the skin, includes fibrillar collagens (mainly collagen I (70%) and III (15%), fibronectin, proteoglycans, and other associated proteins [42, 73]. Cytokines such as TNF α , interleukins, and growth factors such as TGF β , VEGF, FGF, and EGF transcriptionally activate MMPs that control ECM protein degradation and synthesis. Excessive protease activity can lead to a counterproductive chronic healing response, so timed expression and activation of MMPs is essential for burn wound healing [74]. Among proteinases, MMP3 and MMP9 play a role in the degradation of ECM components such as collagen, fibronectin, and elastin following burn wounds, which support dermal repair and regeneration [75, 76]. Our data align with these findings, showing that 4-AP significantly increased the expression of collagen III and I at both gene and protein levels as well as increasing MMP3 and MMP9 expression. This strongly supports a role for 4-AP in ECM repair and regeneration.

In conclusion, our study provides a rationale for a new therapeutic use of 4-AP in treating severe burns and promoting tissue regeneration. 4-AP helps to control inflammation, cell death, and the formation of new blood vessels, which in turn improves the healing of burn wounds by promoting the regrowth of skin and remodeling of underlying tissue. This research could pave the way for further exploration of how 4-AP affects the healing of burns, particularly by looking at the interactions between macrophages and other skin cells such as fibroblasts, endothelial cells, and keratinocytes, which are known to play roles in driving tissue regeneration.

MATERIALS AND METHODS

Vertebrate animals

Ten-week-old C57BL/6J male mice weighing 25 ± 3 g were procured from Jackson Laboratories (Bar Harbor, ME). All animal experiments were approved by the Institutional Animal Care and Use Committee (IACUC; protocol No. 2023-1071) at the University of Arizona College of Medicine in Tucson, AZ.

Mouse model of skin burn injury

Mice were anesthetized by intraperitoneal injection of ketamine hydrochloride (100 mg/kg) and xylazine (10 mg/kg), purchased from Dechra Veterinary Products, KS, USA. The hair was depilated on the thoracolumbar dorsum region using a trimmer followed by hair removal cream (Nads). The skin was prepped for burn wound creation using a 70% alcohol swab (# 5110, Covidien) and 5% povidone-iodine applications (# NDC67618-155-16, Betadine). A full-thickness (third-degree) burn wound was created using a custom-made carbon rod that weighs 65 g (without external pressure) with a 10 mm surface area. The rod was heated to 95 °C using temperature-controlled brass blocks and applied on the animal for 4 seconds (Fig. 1A). Following the burn wound creation, extended-release buprenorphine (3.25 mg/kg, # NDC86084-100-30, Ethiqa XR, Fidelis animal health) was given subcutaneously to all animals as an analgesic. The experimental animals ($n = 6$ animals/group) were randomly assigned to burn wounds (normal saline, 0.1 ml/mouse) and burn wounds with 4-AP (2 mg/kg; # A78403, Millipore Sigma) groups. 4-AP or saline was given intraperitoneally immediately after surgery and post-surgery days 1 to 21. The lowest starting dose of 4-AP in humans for multiple sclerosis is 10 mg once daily, and the calculated body mass-adjusted human equivalent dose of 4-AP in mice is 2 mg/kg [77, 78]. All animals were euthanized using isoflurane anesthesia, followed by cervical dislocation on days 3, 7, and 21. Next, skin samples were harvested to analyze skin histomorphometry, apoptosis, angiogenesis, inflammation, and regeneration or remodeling using immunofluorescence (IF), qRT-PCR, and Western blotting.

Measurement of burn wound closure

Burn wound healing was monitored daily, and burned images were taken using a digital camera on post-injury days 0, 3, 5, 7, 10, 14, 18, and 21 (Fig. 1A). The size of the burn wound areas was measured in pixels using NIH ImageJ-1.53e software (National Institutes of Health, Bethesda, MD, USA) using a reference scale. Wound closure is expressed as a percentage of day 0 wounds using the following formula.

$$\text{Wound closure (\%)} = \frac{(\text{Area of original wound at day 0} - \text{Area of wound at postulated day})}{\text{Area of original wound at day 0}} \times 100$$

Skin tissue processing and histological analysis

Skin tissue processing and hematoxylin and eosin (H & E) staining were performed as described in our previous publication [3]. Briefly, on days 3, 7, and 21, the skin was harvested from the wound bed using a 12 mm biopsy punch (# NC9253254, Fisher Scientific) and then halved at the center of the wound to use histology and gene or protein expression analysis. Next, skin tissues were fixed in 4% paraformaldehyde (# SC281692, ChemCruz) solution overnight, washed with 70% alcohol 3 times, and embedded in paraffin. The serial 5 μ m thick vertical sections were taken from the skin tissues embedded blocks using a microtome (# HM315, GMI). Before staining, tissue sections were deparaffinized and serially rehydrated using xylene and alcohol respectively. The sections were stained with H&E staining kit as per the manufacturer's protocol with slight modifications (# ab245880, Sigma-Aldrich). Briefly, the tissues were stained with modified Mayer's hematoxylin for 5 min and then incubated with a bluing reagent for 15 s. Next, sections were stained with eosin (# 71204, Thermo Scientific) for 20 s, followed by dehydration with 95% and 100% alcohol for 5 min, two times. Sections were then cleared in xylene for 5 min, 2 times, and mounted with DPX mountant (# 06522, Sigma-Aldrich). H & E-stained slides were scanned using a slide scanner (MoticEasyScan, SF, USA) at 80 X magnification.

Immunofluorescence staining and analysis

Skin tissue IF staining was performed as described in our previous publication [16]. Briefly, antigen retrieval was performed using a 10 mM sodium citrate buffer (pH 6.0) for 20 min at 95 °C. Permeabilization and blocking of nonspecific binding were performed using 1% Triton X-100

and 5% goat serum respectively. Next, primary antibody staining was performed with CD31 (1:100, # 553370, BD Pharmingen), IL1 β (1:250, # GTX74034, GeneTex), CD206 (1:400, # 141703, BioLegend), F4/80 (1:500, # SAB4501656, Sigma Aldrich), K10 (1:100, # SAB4501656, Sigma Aldrich), K14 (1:100, # NBP2-34270, Novus Biologicals), Vimentin (1:200, # 10366-1-AP, Thermo Fisher Scientific), and α -SMA (1:500, # 14-9760-82, Thermo Fisher Scientific) at 4 °C overnight incubation. Then, samples were washed thrice with PBS and were incubated with the appropriate secondary antibody: Alexa Fluor 488 (1:1000, # A32723, Invitrogen) and Alexa Fluor 647 (1:1000, # A32733, Invitrogen) for 1 h at room temperature. Staining without primary antibodies was used as a control for nonspecific fluorescence. Nuclei were counter-stained using ProLong™ Gold anti-fade reagent with DAPI (# P36935, Thermo Fisher Scientific) and sections were examined under a fluorescent microscope (# DM6000, Leica, IL, USA). The image analysis and quantification were performed using NIH ImageJ-1.53e software.

Macrophage cell viability assay

Mouse bone marrow-derived macrophage (BMM ϕ) isolation and ex-vivo expansion were performed using our established protocol [79]. Cell viability tests were conducted using the MTT assay ([(3-(4,5-dimethylthiazol-2-yl)-2,5-diphenyltetrazolium bromide)]) (# M5655, Sigma), following the manufacturer's instructions. Briefly, BMM ϕ s were seeded at a concentration of 2×10^4 cells/well in a 96-well plate and incubated for 24 h at 37 °C and 5% CO₂. Cells were treated with different concentrations of 4-AP (1, 10, and 500 nM and 1, 50, 100, 500, 1000, 2000, 4000, and 8000 μ M) for 24 hr. After treatment, the MTT reagent at a final concentration of 0.5 mg/mL was added, and the cells were incubated for 3 hr in a 5% CO₂ incubator. Following incubation, the MTT reagent was removed, and dimethylsulfoxide (DMSO) solubilization solution (# 4-X, ATCC) was added to each well and stirred using a gyratory shaker to dissolve the formazan crystals. The absorbance was measured at 570 nm using a microplate spectrophotometer (Molecular Devices SpectraMax M3, NH, USA) to calculate cell viability percentages. Untreated cells were used as controls.

Macrophage calcium imaging

BMM ϕ s were cultured in a four-well chamber slide (# 155382PK, Nunc Lab Tek) with DMEM complete medium at a density of $\sim 5 \times 10^4$ cells per well and then incubated in a humidified chamber at 37 °C in 5% CO₂ for 24 h. At $\sim 60\%$ confluence, cells were treated with either lipopolysaccharide (LPS, 50 ng/ml) or LPS + 4-AP (1 μ M) or not treated (control group) for 24 h. Next, cells were washed with 1X DPBS and stained with 1X Calbryte 520AM dye (# 20650, AAT Bioquest) for 1 h at 37 °C in 5% CO₂. Afterward, the cells were washed with 1X DPBS, fixed with 4% paraformaldehyde (# J19943.K2, Thermo Fisher Scientific) for 15 min, and coverslips were mounted on glass slides using an antifade mounting medium with DAPI (# P36971, Thermo Fisher Scientific). The calcium expression of BMM ϕ s was imaged using a fluorescent microscope (# DM6000, Leica, IL, USA) and was analyzed using NIH-ImageJ software.

Flowcytometry analysis

Single-cell suspensions of LPS (50 ng/mL) and LPS (50 ng/mL) + 4-AP (1 μ M) treated BMM ϕ s were prepared and washed with ice-cold 1X DPBS [79]. LPS treatment was for 24 hr, whereas 4-AP treatment lasted 48 h. Next, cells were resuspended in 1X flow cytometry staining buffer (# FC001, R&D) and were stained with CD206 (1:100, # 141703, Biolegend) and F4/80 (1:100, # 565411, BD Biosciences) conjugated antibodies for 30 min. After staining, the cells were fixed with 4% paraformaldehyde and resuspended in a staining buffer. The data was acquired using BD FACSDiva™ v7 software and analyzed using FlowJo v10.8 Software.

TUNEL staining

To examine burned skin cell death or apoptosis, a terminal deoxynucleotidyl transferase dUTP nick end labeling (TUNEL) assay kit (HRP-DAB method) (# ab206386, Abcam) was used according to the manufacturer's protocol. The process involved the following steps: 1. Deparaffinization of paraffin-embedded skin tissue sections using xylene, followed by serial rehydration in alcohol. 2. Treating with proteinase-K for 20 min at room temperature. 3. Washing with tris-buffered saline (TBS) and incubating in 30% H₂O₂ in methanol for 5 min at room temperature. 4. Washing with TBS buffer and incubating in terminal deoxynucleotidyl transferase (TdT) equilibration buffer for 30 min at room temperature. 5. Incubation in the

TdT labeling reaction mixture for 90 min at 37 °C in a humidified chamber. 6. Washing in a TBS buffer, addition of stop buffer, and incubation for 5 min at room temperature, followed by blocking buffer incubation for 10 min. 7. Wash off the blocking buffer and incubate the slides in 1X conjugate for 30 min at room temperature. 8. Subsequent washing with TBS, staining with 3,3'-diaminobenzidine (DAB) solution, and incubation at room temperature for 15 min. 9. Washing with distilled water to remove unbound DAB, then counter-staining the nuclei with methyl green and mounting with DPX mountant (# 0622, Sigma). Finally, slides were imaged using a slide scanner (MoticEasyScan, SF, USA) at 80 X magnification.

RNA extraction and qRT-PCR analysis

Total RNA was extracted from the skin tissues and BMMØs (Groups: Control-no treatment, LPS-50 ng/mL and LPS + 4-AP-1 µM) using the RNeasy kit (# 74104, Qiagen). LPS treatment was for 24 h, whereas 4-AP treatment lasted 48 h. An equal amount of RNA (1000 ng) was reverse transcribed to cDNA using a high-capacity reverse transcription kit (# 4368814, Applied Biosystems). The primers (Invitrogen, Life Technologies) are detailed in the Supplementary Table S1. qRT-PCR gene expression analysis was performed using Fast SYBR Green Master Mix (# 4367659, Applied Biosystems) with a Real-Time PCR System (Azure Cielo 6) [80]. The relative mRNA expression of the targeted genes was normalized against the glyceraldehyde 3-phosphate dehydrogenase (GAPDH) gene. The data were represented as fold change with 4-AP versus saline.

Protein extraction and Western blotting analysis

Skin sample protein extraction was performed using T-PER™ extraction reagent (# 78510, Thermo Fisher Scientific). Briefly, the samples were homogenized at 4 °C using 0.9–2.0 mm stainless steel beads (# SSB14B, Next Advance) at 5000 rpm for 5 min, followed by 13000 rpm for 20 min using a bullet blender (# BBX24, Next Advance Homogenizer). BMMØs total protein extraction was performed using RIPA lysis extraction reagent (# R0278, Sigma). The extracted protein was quantified using a BCA assay kit (# 23225, Thermo Fisher Scientific). To identify targeted proteins, 20 to 50 µg of the isolated protein samples were loaded and separated using 4–12% sodium dodecyl sulfate-polyacrylamide gel electrophoresis (# 4561044, GenScript). The gel was then transferred to a polyvinylidene fluoride (PVDF) membrane by wet transfer system (# L00686, GenScript) and blocked with 3% BSA in 1X TBST for 1 h at 37 °C. The membrane was then incubated in the primary antibody overnight at 4 °C. The primary antibodies used are mouse IL-1β (1: 500, # GTX74034, Genetex), CD206 (1:400, # 141703, BioLegend), ARG-1 (1:2000, # 93668 s, Cell Signaling), Orai1 (1:1000, # PA5-26378, Thermo Fisher), pSTAT6 (1:1000, # 56554S, Cell Signaling Technology), VEGF (1:1000, # JH121, Invitrogen), CD31, 1:1000, # 553370, BD Pharmingen), eNOS (1:2000, # 32027 s, Cell Signaling), BAX (1:2000, # 14796, Cell Signaling), BCL2 (1:2000, # 4223, Cell Signaling), BCL-XL (1:2000, # 2764 s, Cell Signaling), K10 (1:2000, # SAB4501656, Sigma Aldrich), K14 (1:5000, # NBP2-34270, Novus Biologicals), TGFβ (1:1000, # 3711 s, Cell Signaling), Vimentin (1:5000, # 10366-1-AP, Thermo Fisher Scientific), α-SMA (1:500, # 14-9760-82, Thermo Fisher Scientific), and GAPDH (1:5000, # MA5-15738, Thermo Fisher Scientific). The membranes were then washed thrice with the tris buffered saline with Tween 20 (TBST) buffer and incubated with the respective secondary antibodies. The secondary antibodies used are an anti-rabbit HRP-linked antibody (# 7074, Cell signaling) and an anti-mouse HRP-linked antibody (# 7076, Cell signaling). The blots were developed using Super Signal West Pico PLUS chemiluminescent substrate ECL kit (# 34579, Thermo Fisher Scientific), and images were captured using a G-box ChemiXRQ gel imager. The bands were quantified using NIH ImageJ-1.53e software. All uncut original Western blotting images of targeted proteins are available in the supplemental material.

Collagen staining and analysis

The skin collagen staining was performed using Herovici's collagen staining kit (# KTHER, StatLab). Briefly, the deparaffinized slides were immersed in Weigert's hematoxylin for 5 min and then rinsed in running tap water for 45 s. Next, the tissues were stained with Herovici's working solution for 2 min, followed by 1% acetic acid for 2 min. The slides were then dehydrated in absolute alcohol and cleared in xylene, each for 1 min, three times. Finally, the slides were mounted using organic mountant (# 06522, Sigma Aldrich). The images were captured at 80 X magnification using a slide scanner (MoticEasyScan, SF, USA) and analyzed using NIH ImageJ-1.53e software.

Statistical analysis

All data were analyzed using GraphPad Prism Version 10.1.1 (San Diego, USA). Comparisons between two groups with $n \geq 3$ were conducted using two-tailed, unpaired t-tests. Ordinary one-way analysis of variance (ANOVA) was utilized to compare three groups with $n \geq 3$. All values are presented as mean \pm SEM. Significance levels (P-values < 0.05) were documented using standard symbols (*, **, and *** correspond to $P < 0.05$, $P < 0.0021$, and $P < 0.0002$, respectively).

DATA AVAILABILITY

Data in the main text and the supplementary information are available from the corresponding authors upon reasonable request. The data presented in this study are available on request from the corresponding author.

REFERENCES

1. Jeschke MG, van Baar ME, Choudhry MA, Chung KK, Gibran NS, Logsetty S. Burn injury. *Nat Rev Dis Prim.* 2020;6:11.
2. Ivanko A, Garbuzov AE, Schoen JE, Kearns R, Phillips B, Murata E, et al. The Burden of Burns: An Analysis of Public Health Measures. *J Burn Care Res.* 2024. <https://doi.org/10.1093/jbcr/rae053>.
3. Ivanko A, Garbuzov A, Schoen JE, Kearns RD, Danos D, Murata E, et al. 101 The Burden of Burns: An Analysis of Public Health Measures. *J Burn Care Res.* 2024;45:82–82.
4. Schaefer TJ, Tannan SC. Thermal Burns. In: *StatPearls.* StatPearls Publishing: Treasure Island (FL), 2024. <http://www.ncbi.nlm.nih.gov/books/NBK430773/> (accessed 18 Jun2024).
5. Warby R, Maani CV. Burn Classification. In: *StatPearls.* StatPearls Publishing: Treasure Island (FL), 2024. <http://www.ncbi.nlm.nih.gov/books/NBK539773/> (accessed 18 Jun2024).
6. Żwierello W, Piorun K, Skórka-Majewicz M, Maruszewska A, Antoniewski J, Gutowska I. Burns: Classification, Pathophysiology, and Treatment: A Review. *Int J Mol Sci.* 2023;24:3749.
7. Sierawska O, Małkowska P, Taskin C, Hrynkiewicz R, Mertowska P, Grywalska E, et al. Innate Immune System Response to Burn Damage-Focus on Cytokine Alteration. *Int J Mol Sci.* 2022;23:716.
8. Penatzer JA, Srinivas S, Thakkar RK. The role of macrophages in thermal injury. *Int J Burns Trauma.* 2022;12:1–12.
9. Strudwick XL, Cowin AJ. The Role of the Inflammatory Response in Burn Injury. In: Kartal SP, Bayramgürler D (eds). *Hot Topics in Burn Injuries.* InTech, 2018. <https://doi.org/10.5772/intechopen.71330>.
10. Sim SL, Kumari S, Kaur S, Khosroehrani K. Macrophages in Skin Wounds: Functions and Therapeutic Potential. *Biomolecules.* 2022;12:1659.
11. Wang ECE, Dai Z, Ferrante AW, Drake CG, Christiano AM. A Subset of TREM2+ Dermal Macrophages Secretes Oncostatin M to Maintain Hair Follicle Stem Cell Quiescence and Inhibit Hair Growth. *Cell Stem Cell.* 2019;24:654–69.e6.
12. Castellana D, Paus R, Perez-Moreno M. Macrophages contribute to the cyclic activation of adult hair follicle stem cells. *PLoS Biol.* 2014;12:e1002002.
13. Lucas T, Waisman A, Ranjan R, Roes J, Krieg T, Müller W, et al. Differential roles of macrophages in diverse phases of skin repair. *J Immunol.* 2010;184:3964–77.
14. Radzikowska-Büchner E, Łopuszyńska I, Flieger W, Tobiasz M, Maciejewski R, Flieger J. An Overview of Recent Developments in the Management of Burn Injuries. *Int J Mol Sci.* 2023;24:16357.
15. Davis FA, Stefoski D, Rush J. Orally administered 4-aminopyridine improves clinical signs in multiple sclerosis. *Ann Neurol.* 1990;27:186–92.
16. Jagadeeshwaraprasad MG, Govindappa PK, Nelson AM, Noble MD, Elfar JC. 4-Aminopyridine Induces Nerve Growth Factor to Improve Skin Wound Healing and Tissue Regeneration. *Biomedicines.* 2022;10:1649.
17. Elfar J. 4-aminopyridine for Skin Wound Healing. <https://clinicaltrials.gov/study/NCT06333171>.
18. Bonsignore G, Martinotti S, Ranzato E. Wound Repair and Ca²⁺ Signalling Interplay: The Role of Ca²⁺ Channels in Skin. *Cells.* 2024;13:491.
19. Vandenberghe M, Raphaël M, Lehen'kyi V, Gordienko D, Hastie R, Oddos T, et al. ORAI1 calcium channel orchestrates skin homeostasis. *Proc Natl Acad Sci USA.* 2013;110:E4839–48.
20. Abdullahi A, Amini-Nik S, Jeschke MG. Animal models in burn research. *Cell Mol Life Sci.* 2014;71:3241–55.
21. Burgess M, Valdera F, Varon D, Kankuri E, Nuutila K. The Immune and Regenerative Response to Burn Injury. *Cells.* 2022;11:3073.
22. Chaker SC, Saad M, Mayes T, Lineaweaver WC. Burn Injury-related Growth Factor Expressions and Their Potential Roles in Burn-related Neuropathies. *J Burn Care Res.* 2024;45:25–31.

23. Nascimento Da Conceicao V, Sun Y, Ramachandran K, Chauhan A, Raveendran A, Venkatesan M, et al. Resolving macrophage polarization through distinct Ca^{2+} entry channel that maintains intracellular signaling and mitochondrial bioenergetics. *iScience*. 2021;24:103339.

24. Nascimento Da Conceicao V, Sun Y, Zboril EK, De la Chapa JJ, Singh BB. Loss of Ca^{2+} entry via Orai-TRPC1 induces ER stress, initiating immune activation in macrophages. *J Cell Sci*. 2019;133:jcs237610.

25. Sindhuvarak A, Mishra AM, Gupta D, Iaci JF, Parry TJ, Carmel JB. Clinically Relevant Levels of 4-Aminopyridine Strengthen Physiological Responses in Intact Motor Circuits in Rats, Especially After Pyramidal Tract Injury. *Neurorehabil Neural Repair*. 2017;31:387–96.

26. Clark AR, Hsu CG, Talukder MAH, Noble M, Elfar JC. Transdermal delivery of 4-aminopyridine accelerates motor functional recovery and improves nerve morphology following sciatic nerve crush injury in mice. *Neural Regen Res*. 2020;15:136–44.

27. Shen H, Ma Y, Qiao Y, Zhang C, Chen J, Zhang R. Application of Deferoxamine in Tissue Regeneration Attributed to Promoted Angiogenesis. *Molecules*. 2024;29:2050.

28. Shi Z, Yao C, Shui Y, Li S, Yan H. Research progress on the mechanism of angiogenesis in wound repair and regeneration. *Front Physiol*. 2023;14:1284981.

29. Rennekampff H-O, Alharbi Z. Burn Injury: Mechanisms of Keratinocyte Cell Death. *Med Sci (Basel)*. 2021;9:51.

30. Bhatia A, O'Brien K, Chen M, Wong A, Garner W, Woodley DT, et al. Dual therapeutic functions of F-5 fragment in burn wounds: preventing wound progression and promoting wound healing in pigs. *Mol Ther Methods Clin Dev*. 2016;3:16041.

31. Singer AJ, Boyce ST. Burn Wound Healing and Tissue Engineering. *J Burn Care Res*. 2017;38:e605–e613.

32. Guo H, Xing Y, Deng F, Yang K, Li Y. Secreted Frizzled-related protein 4 inhibits the regeneration of hair follicles. *PeerJ*. 2019;6:e6153.

33. Hammond NL, Headon DJ, Dixon MJ. The cell cycle regulator protein 14-3- σ is essential for hair follicle integrity and epidermal homeostasis. *J Invest Dermatol*. 2012;132:1543–53.

34. Darby IA, Laverdet B, Bonté F, Desmoulière A. Fibroblasts and myofibroblasts in wound healing. *Clin Cosmet Investig Dermatol*. 2014;7:301–11.

35. Hermanns-Lê T, Piérard GE, Jennes S, Piérard-Franchimont C. Protomyofibroblast Pathway in Early Thermal Burn Healing. *Ski Pharm Physiol*. 2015;28:250–4.

36. Alhajj M, Goyal A. Physiology, Granulation Tissue. In: *StatPearls*. StatPearls Publishing: Treasure Island (FL), 2024. <http://www.ncbi.nlm.nih.gov/books/NBK554402/> (accessed 18 Jun 2024).

37. Moretti L, Stalfort J, Barker TH, Abebayehu D. The interplay of fibroblasts, the extracellular matrix, and inflammation in scar formation. *J Biol Chem*. 2022;298:101530.

38. Tracy LE, Minasian RA, Caterson EJ. Extracellular Matrix and Dermal Fibroblast Function in the Healing Wound. *Adv Wound Care (N. Rochelle)*. 2016;5:119–36.

39. Lu P, Takai K, Weaver VM, Werb Z. Extracellular matrix degradation and remodeling in development and disease. *Cold Spring Harb Perspect Biol*. 2011;3:a005058.

40. Quan T, Fisher GJ. Role of Age-Associated Alterations of the Dermal Extracellular Matrix Microenvironment in Human Skin Aging: A Mini-Review. *Gerontology*. 2015;61:427–34.

41. Mathew-Steiner SS, Roy S, Sen CK. Collagen in Wound Healing. *Bioeng (Basel)*. 2021;8:63.

42. Diller RB, Tabor AJ. The Role of the Extracellular Matrix (ECM) in Wound Healing: A Review. *Biomim (Basel)*. 2022;7:87.

43. Peña OA, Martin P. Cellular and molecular mechanisms of skin wound healing. *Nat Rev Mol Cell Biol*. <https://doi.org/10.1038/s41580-024-00715-1> 2024.

44. Anderton H, Alqudah S. Cell death in skin function, inflammation, and disease. *Biochem J*. 2022;479:1621–51.

45. Sharifiaghdam M, Shaabani E, Faridi-Majidi R, De Smedt SC, Braeckmans K, Fraire JC. Macrophages as a therapeutic target to promote diabetic wound healing. *Mol Ther*. 2022;30:2891–908.

46. Numaga-Tomita T, Putney JW. Role of STIM-1 and Orai1-mediated Ca^{2+} entry in Ca^{2+} -induced epidermal keratinocyte differentiation. *J Cell Sci*. 2013;126:605–12.

47. Manning D, Dart C, Evans RL. Store-operated calcium channels in skin. *Front Physiol*. 2022;13:1033528.

48. Barreiro O, Cibrán D, Clemente C, Alvarez D, Moreno V, Valiente I, et al. Pivotal role for skin transendothelial radio-resistant anti-inflammatory macrophages in tissue repair. *Elife*. 2016;5:e15251.

49. Barrientos S, Stojadinovic O, Golinko MS, Brem H, Tomic-Canic M. Growth factors and cytokines in wound healing. *Wound Repair Regen*. 2008;16:585–601.

50. Werner S, Grose R. Regulation of wound healing by growth factors and cytokines. *Physiol Rev*. 2003;83:835–70.

51. Johnson KE, Wilgus TA. Vascular Endothelial Growth Factor and Angiogenesis in the Regulation of Cutaneous Wound Repair. *Adv Wound Care (N. Rochelle)*. 2014;3:647–61.

52. Skuli N, Majmundar AJ, Krock BL, Mesquita RC, Mathew LK, Quinn ZL, et al. Endothelial HIF-2 α regulates murine pathological angiogenesis and revascularization processes. *J Clin Invest*. 2012;122:1427–43.

53. Koh TJ, DiPietro LA. Inflammation and wound healing: the role of the macrophage. *Expert Rev Mol Med*. 2011;13:e23.

54. Shaabani E, Sharifiaghdam M, Faridi-Majidi R, De Smedt SC, Braeckmans K, Fraire JC. Gene therapy to enhance angiogenesis in chronic wounds. *Mol Ther Nucleic Acids*. 2022;29:871–99.

55. Peach CJ, Mignone VW, Arruda MA, Alcobia DC, Hill SJ, Kilpatrick LE, et al. Molecular Pharmacology of VEGF-A Isoforms: Binding and Signalling at VEGFR2. *Int J Mol Sci*. 2018;19:1264.

56. Zachary I, Glikl G. Signaling transduction mechanisms mediating biological actions of the vascular endothelial growth factor family. *Cardiovasc Res*. 2001;49:568–81.

57. Shams F, Moravvej H, Hosseinzadeh S, Mostafavi E, Bayat H, Kazemi B, et al. Overexpression of VEGF in dermal fibroblast cells accelerates the angiogenesis and wound healing function: in vitro and in vivo studies. *Sci Rep*. 2022;12:18529.

58. Lecomte K, Toniolo A, Hoste E. Cell death as an architect of adult skin stem cell niches. *Cell Death Differ*. 2024. <https://doi.org/10.1038/s41418-024-01297-3>.

59. Green DR, Llambi F. Cell Death Signaling. *Cold Spring Harb Perspect Biol*. 2015;7:a006080.

60. Khosravi-Far R, Esposti MD. Death receptor signals to mitochondria. *Cancer Biol Ther*. 2004;3:1051–7.

61. Kale J, Osterlund EJ, Andrews DW. BCL-2 family proteins: changing partners in the dance towards death. *Cell Death Differ*. 2018;25:65–80.

62. Shamas-Din A, Kale J, Leber B, Andrews DW. Mechanisms of action of Bcl-2 family proteins. *Cold Spring Harb Perspect Biol*. 2013;5:a008714.

63. Vizely K, Wagner KT, Mandl S, Gustafson D, Fish JE, Radisic M. Angiopoietin-1 derived peptide hydrogel promotes molecular hallmarks of regeneration and wound healing in dermal fibroblasts. *iScience*. 2023;26:105984.

64. Larouche J, Sheoran S, Maruyama K, Martino MM. Immune Regulation of Skin Wound Healing: Mechanisms and Novel Therapeutic Targets. *Adv Wound Care (N. Rochelle)*. 2018;7:209–31.

65. Krzyszczyk P, Schloss R, Palmer A, Berthiaume F. The Role of Macrophages in Acute and Chronic Wound Healing and Interventions to Promote Pro-wound Healing Phenotypes. *Front Physiol*. 2018;9:419.

66. Pastar I, Stojadinovic O, Yin NC, Ramirez H, Nusbaum AG, Sawaya A, et al. Epithelialization in Wound Healing: A Comprehensive Review. *Adv Wound Care (N. Rochelle)*. 2014;3:445–64.

67. Villarreal-Ponce A, Tiruneh MW, Lee J, Guerrero-Juarez CF, Kuhn J, David JA, et al. Keratinocyte-Macrophage Crosstalk by the Nrf2/Ccl2/EGF Signaling Axis Orchestrates Tissue Repair. *Cell Rep*. 2020;33:108417.

68. Donetti E, Lombardo G, Indino S, Cornaghi L, Arnaboldi F, Pescitelli L, et al. The psoriatic shift induced by interleukin 17 is promptly reverted by a specific anti-IL-17A agent in a three-dimensional organotypic model of normal human skin culture. *Eur J Histochem*. 2020;64:3115.

69. DiTommaso T, Cottle DL, Pearson HB, Schlüter H, Kaur P, Humbert PO, et al. Keratin 76 is required for tight junction function and maintenance of the skin barrier. *PLoS Genet*. 2014;10:e1004706.

70. Alam H, Sehgal L, Kundu ST, Dalal SN, Vaidya MM. Novel function of keratins 5 and 14 in proliferation and differentiation of stratified epithelial cells. *Mol Biol Cell*. 2011;22:4068–78.

71. Zhang L. Keratins in Skin Epidermal Development and Diseases. In: Blumenberg M (ed). *Keratin*. IntechOpen, 2018. <https://doi.org/10.5772/intechopen.79050>.

72. Li X, Xie R, Luo Y, Shi R, Ling Y, Zhao X, et al. Cooperation of TGF- β and FGF signalling pathways in skin development. *Cell Prolif*. 2023;56:e13489.

73. Widgerow AD, Fabi SG, Palestine RF, Rivkin A, Ortiz A, Bucay VW, et al. Extracellular Matrix Modulation: Optimizing Skin Care and Rejuvenation Procedures. *J Drugs Dermatol*. 2016;15:s63–71.

74. Caley MP, Martins VLC, O'Toole EA. Metalloproteinases and Wound Healing. *Adv Wound Care (N. Rochelle)*. 2015;4:225–34.

75. Van Doren SR. Matrix metalloproteinase interactions with collagen and elastin. *Matrix Biol*. 2015;44–46:224–31.

76. Bigg HF, Rowan AD, Barker MD, Cawston TE. Activity of matrix metalloproteinase-9 against native collagen types I and III. *FEBS J*. 2007;274:1246–55.

77. Goodman AD, Brown TR, Cohen JA, Krupp LB, Schapiro R, Schwid SR, et al. Dose comparison trial of sustained-release fampridine in multiple sclerosis. *Neurology*. 2008;71:1134–41.

78. Nair A, Morsy MA, Jacob S. Dose translation between laboratory animals and human in preclinical and clinical phases of drug development. *Drug Dev Res*. 2018;79:373–82.

79. Govindappa PK, Elfar JC. Erythropoietin promotes M2 macrophage phagocytosis of Schwann cells in peripheral nerve injury. *Cell Death Dis*. 2022;13:245.

80. Ellur G, Sukhdeo SV, Khan MT, Sharan K. Maternal high protein-diet programs impairment of offspring's bone mass through miR-24-1-5p mediated targeting of SMAD5 in osteoblasts. *Cell Mol Life Sci*. 2021;78:1729–44.

ACKNOWLEDGEMENTS

The authors acknowledge The University of Arizona College of Medicine, Tucson, AZ, USA, for supporting this study.

AUTHOR CONTRIBUTIONS

RVG (animal surgery assistance, dosing, tissue collection, processing, and experiments, data acquisition, analysis, and interpretation, and figure generation and finalization); GE (animal surgery assistance, imaging, tissue collection, processing, and experiments, data acquisition, analysis, and interpretation, and figure generation and finalization); AAG (animal surgery assistance, imaging, and data organization); PKG (concept and design of the study, animal surgery, data analysis, and interpretation, figure finalization, and manuscript drafting); JCE (concept and design of the study, data interpretation, manuscript finalization, and funding acquisition). All authors read and approved the final manuscript.

FUNDING

This work was supported by grants from the National Institutes of Health (NIH; K08 AR060164-01A) and U.S. Department of Defense (DOD; W81XWH-16-1-0725) to JCE, in addition to institutional support from The University of Arizona College of Medicine, Tucson, AZ, USA. The funding bodies played no role in the design of the study and collection, analysis, interpretation of data, and in writing the manuscript.

COMPETING INTERESTS

PKG and JCE are inventors on patents 1). Methods and materials for treating burns (US18/139,123); 2). Methods and materials for treating hair loss (US18/270,914); 3). Methods and materials for treating nerve injury and/or promoting wound healing (US17/759,224) submitted by the Penn State Research Foundation. All other authors declare that they have no competing financial interests.

ETHICAL APPROVAL

Our manuscript does not contain any human data. Experimental design and animal protocols were approved by the Institutional Animal Care and Use Committee (IACUC) at The University of Arizona College of Medicine, Tucson, AZ. All experiments were conducted in accordance with the approved guidelines and regulations.

ADDITIONAL INFORMATION

Supplementary information The online version contains supplementary material available at <https://doi.org/10.1038/s41420-024-02199-6>.

Correspondence and requests for materials should be addressed to Prem Kumar Govindappa or John C. Elfar.

Reprints and permission information is available at <http://www.nature.com/reprints>

Publisher's note Springer Nature remains neutral with regard to jurisdictional claims in published maps and institutional affiliations.



Open Access This article is licensed under a Creative Commons Attribution 4.0 International License, which permits use, sharing, adaptation, distribution and reproduction in any medium or format, as long as you give appropriate credit to the original author(s) and the source, provide a link to the Creative Commons licence, and indicate if changes were made. The images or other third party material in this article are included in the article's Creative Commons licence, unless indicated otherwise in a credit line to the material. If material is not included in the article's Creative Commons licence and your intended use is not permitted by statutory regulation or exceeds the permitted use, you will need to obtain permission directly from the copyright holder. To view a copy of this licence, visit <http://creativecommons.org/licenses/by/4.0/>.

© The Author(s) 2024